Research Article | Vol. 26, No. 4 | 19 Feb 2018 | OPTICS EXPRESS 3882

Optics EXPRESS

Anti-stiction coating for mechanically tunable photonic crystal devices

M. PETRUZZELLA,[1,3,*] Ž. ZOBENICA,[1,3] M. COTRUFO,[1] V. ZARDETTO,[1] A. MAMELI,[1] F. PAGLIANO,[1,2] S. KOELLING,[1] F. W. M. VAN OTTEN,[1] F. ROOZEBOOM,[1] W. M. M. KESSELS,[1] R. W. VAN DER HEIJDEN,[1] AND A. FIORE[1]

[1]*Department of Applied Physics and Institute for Photonic Integration, Eindhoven University of Technology, Eindhoven, The Netherlands*
[2]*nanoPHAB B.V. Eindhoven, The Netherlands*
[3]*These authors contributed equally to the work*
[*]*m.petruzzella@tue.nl*

Abstract: A method to avoid the stiction failure in nano-electro-opto-mechanical systems has been demonstrated by coating the system with an anti-stiction layer of Al_2O_3 grown by atomic layer deposition techniques. The device based on a double-membrane photonic crystal cavity can be reversibly operated from the pull-in back to its release status. This enables to electrically switch the wavelength of a mode over ~50 nm with a potential modulation frequency above 2 MHz. These results pave the way to reliable nano-mechanical sensors and optical switches.

OCIS codes: (050.5298) Photonic crystals; (230.4685) Optical microelectromechanical devices.

References and links

1. F. Chollet, "Devices based on co-integrated MEMS actuators and optical waveguide: A review," Micromachines (Basel) **7**(2), 18 (2016).
2. H. Du, F. S. Chau, and G. Zhou, "Mechanically-Tunable Photonic Devices with On-Chip Integrated MEMS/NEMS Actuator," Micromachines (Basel) **7**(4), 69 (2016).
3. C. P. Dietrich, A. Fiore, M. G. Thompson, M. Kamp, and S. Höfling, "GaAs integrated quantum photonics: Towards compact and multi-functional quantum photonic integrated circuits," Laser Photonics Rev. **10**(6), 870–894 (2016).
4. L. Midolo, F. M. Pagliano, T. B. Hoang, T. Xia, F. W. van Otten, L. H. Li, E. H. Linfield, M. Lermer, S. Höfling, and A. Fiore, "Spontaneous emission control of single quantum dots by electromechanical tuning of a photonic crystal cavity," Appl. Phys. Lett. **101**(9), 091106 (2012).
5. M. Petruzzella, T. Xia, F. M. Pagliano, S. Birindelli, L. Midolo, Z. Zobenica, L. H. Li, E. H. Linfield, and A. Fiore, "Fully tuneable, Purcell-enhanced solid-state quantum emitters," Appl. Phys. Lett. **107**(14), 141109 (2015).
6. P. Lodahl, S. Mahmoodian, and S. Stobbe, "Interfacing single photons and single quantum dots with photonic nanostructures," Rev. Mod. Phys. **87**(2), 347–400 (2015).
7. R. Perahia, J. D. Cohen, S. Meenehan, T. M. Alegre, and O. Painter, "Electrostatically tunable optomechanical "zipper" cavity laser," Appl. Phys. Lett. **97**(19), 191112 (2010).
8. I. W. Frank, P. B. Deotare, M. W. McCutcheon, and M. Lončar, "Programmable photonic crystal nanobeam cavities," Opt. Express **18**(8), 8705–8712 (2010).
9. X. Chew, G. Zhou, F. S. Chau, J. Deng, X. Tang, and Y. C. Loke, "Dynamic tuning of an optical resonator through MEMS-driven coupled photonic crystal nanocavities," Opt. Lett. **35**(15), 2517–2519 (2010).
10. L. Midolo, S. N. Yoon, F. Pagliano, T. Xia, F. W. van Otten, M. Lermer, S. Höfling, and A. Fiore, "Electromechanical tuning of vertically-coupled photonic crystal nanobeams," Opt. Express **20**(17), 19255–19263 (2012).
11. L. Midolo, P. J. van Veldhoven, M. A. Dündar, R. Nötzel, and A. Fiore, "Electromechanical wavelength tuning of double-membrane photonic crystal cavities," Appl. Phys. Lett. **98**(21), 211120 (2011).
12. L. Midolo and A. Fiore, "Design and optical properties of electromechanical double-membrane photonic crystal cavities," IEEE J. Quantum Electron. **50**(6), 404–414 (2014).
13. W. M. Zhang, H. Yan, Z. K. Peng, and G. Meng, "Electrostatic pull-in instability in MEMS/NEMS: A review," Sens. Actuators A Phys. **214**, 187–218 (2014).
14. R. Maboudian, W. R. Ashurst, and C. Carraro, "Self-assembled monolayers as anti-stiction coatings for MEMS: characteristics and recent developments," Sens. Actuators A Phys. **82**(1–3), 219–223 (2000).

#309205 https://doi.org/10.1364/OE.26.003882
Journal © 2018 Received 25 Oct 2017; revised 18 Jan 2018; accepted 18 Jan 2018; published 6 Feb 2018

Optics EXPRESS

15. F. W. DelRio, C. F. Herrmann, N. Hoivik, S. M. George, V. M. Bright, J. L. Ebel, R. E. Strawser, R. Cortez, and K. D. Leedy, "Atomic layer deposition of Al_2O_3/ZnO nano-scale films for gold RF MEMS," Microwave Symposium Digest, I.E.E.E. M.T.T.S. Int. Microw. Symp. **3**, 1923–1926 (2004).
16. N. D. Hoivik, J. W. Elam, R. J. Linderman, V. M. Bright, S. M. George, and Y. C. Lee, "Atomic layer deposited protective coatings for micro-electromechanical systems," Sens. Actuators A Phys. **103**(1–2), 100–108 (2003).
17. G. Dingemans and W. M. M. Kessels, "Status and prospects of Al_2O_3-based surface passivation schemes for silicon solar cells," J. Vac. Sci. Technol. A **30**(4), 040802 (2012).
18. S. Kiravittaya, H. S. Lee, L. Balet, L. H. Li, M. Francardi, A. Gerardino, A. Fiore, A. Rastelli, and O. G. Schmidt, "Tuning optical modes in slab photonic crystal by atomic layer deposition and laser-assisted oxidation," J. Appl. Phys. **109**(5), 053115 (2011).
19. T. Süss, P. Braeuninger-Weimer, and C. Hierold, "Stress reduction in ultra-small thin film Al_2O_3 diaphragms by atomic layer deposition," Sens. Actuators A Phys. **212**, 159–164 (2014).
20. Ž. Zobenica, R. W. van der Heijden, M. Petruzzella, F. Pagliano, R. Leijssen, T. Xia, L. Midolo, M. Cotrufo, Y. Cho, F. W. M. van Otten, E. Verhagen, and A. Fiore, "Integrated nano-opto-electro-mechanical sensor for spectrometry and nanometrology," Nat. Commun. **8**(1), 2216 (2017).

1. Introduction

Nano-opto-electro-mechanical-systems (NOEMS) represent an attractive platform to build a novel class of reconfigurable photonic devices such as tunable filters, optical accelerometers, spectrometers, switches and adaptive waveguides [1]. Their combination with photonic crystals (PhC) allows the control of the frequencies of optical modes without introducing additional losses [2]. For this reason, their use has attracted attention in quantum photonic integrated circuits [3], for instance to control the relative detuning between cavities and emitters [4, 5] or to enhance the light-matter interaction [6].

A promising approach for controlling the emission of nano-resonators over a wide wavelength range consists in altering the evanescent coupling of two strongly-coupled nanocavities by the mechanical movement of one resonator with respect to the other. This leads to an opposite and reversible energy shift of the super-modes of the system. This concept has been implemented using laterally- [7–9] and vertically- [10] coupled PhC nanobeams and parallel two-dimensional PhC membranes [11].

However, despite their potential, the reliability and performance of these devices is often compromised by the combination of the pull-in instability [13] and surface forces, which can lead to a permanent stiction between two movable mechanical elements. The pull-in instability occurs when the distance between two movable parts is reduced below 2/3 of its original value upon the action of a constant voltage. Above this threshold, the electrostatic force overcomes the restoring elastic force of the system, resulting in an abrupt transition that brings the movable elements into contact. The latter can adhere permanently due to short-range interactions that include van der Waals and capillary forces. For these reasons, pull-in and stiction failure has represented one of the major drawbacks in the use of MEMS and NEMS for real-life applications. Several solutions to this problem have been proposed for micro-actuators such as the use of self-assembled monolayers [14] and the deposition of dielectric layers [15, 16], but they have not been explored so far in the context of NOEMS. Importantly, due to the very short distance (100-200 nm) between the moving parts of this class of devices, the application of anti-stiction layers can be very challenging, and may produce a degradation of their mechanical and optical properties.

In this work, we present a method to avoid the permanent adhesion of two active photonic crystal nano-membranes. This method is based on the conformal deposition of a thin layer of alumina via atomic layer deposition (ALD), which prevents the direct contact between the doped regions of the membranes composing the NOEMS. We show the effect of this dielectric layer on the optical and mechanical properties of this tunable PhC cavity when it is operated statically and dynamically. Besides allowing the reliable recovery from pull-in, this enables the use of the device as a switch between two widely different optical/mechanical states.

Optics EXPRESS

2. Device concept and protective ALD coating

The device under study consists of two GaAs photonic crystal membranes, as illustrated in Fig. 1(a). These two slabs have identical thicknesses (t = 170 nm) and are separated along the vertical direction by a small air gap of d_0 = 200 nm. The initial inter-membrane gap (d) can be reduced electromechanically by biasing a p-i-n diode fabricated across the two membranes. To this end, the bottom part of the top membrane and the upper part of the bottom membrane are n- and p-doped, respectively. When the diode is operated in reverse bias, charges accumulate in the two doped regions and the system behaves as a capacitor. While the bottom membrane is clamped from all sides and can thus be considered as fixed, the upper membrane - patterned as a micro-bridge- is free to move under the application of an electrostatic potential. Further fabrication details can be found in [12].

The system can be described within the coupled-mode theory framework. In particular, the field distribution can be approximately factorized in two independent functions: an in-plane component that depends on the actual photonic crystal layout, and a vertical field distribution associated with the effective refractive index (n_{eff}) of the structure. Due to the small distance between the membranes, the single-membrane guided modes split in symmetric (s) and anti-symmetric (as) vertical super-modes having a higher and a lower effective refractive index, respectively. The membrane movement modulates the evanescent coupling between the two slabs and, consequently, the effective refractive index of the super-modes and the PhC resonances (Fig. 1(c)). The mode wavelengths therefore represent a unique fingerprint of the mechanical status of the NOEMS, and can be exploited to derive the properties of the NOEMS during static and dynamic actuation experiments.

A layer of self-assembled high-density quantum dots is grown in the middle of the top membrane and is employed as an internal source to excite the photonic modes of the structure. The cavity design is a standard L3 cavity, i.e. three consecutive holes are removed from a hexagonal hole lattice. In the following experiments, a 15-nm alumina (Al_2O_3) layer has been deposited in a standard ALD reactor employing trimethyl aluminum (TMA) as a precursor and O_2 plasma as reactant [17]. Alumina is expected to avoid short-cuts between the doped layers of the device and has been used before as anti-stiction layer in polysilicon MEMS [16]. The flux of O_2 is maintained constant for the entire duration of the process at a pressure p = 7.5 x 10^{-3} mbar. The deposition is conducted close to room-temperature (T = 60 °C) and consists of 100 cycles. Each cycle is composed of the following steps: (i) dosing precursor TMA (30 ms); (ii) purging for 3 s; (iii) O_2 plasma for 3 s at a power P = 100 W; (iv) purging for 3 s.We present the effect of the coating on three distinct devices labelled A, B, and C, having nominally identical mechanical properties and lattice constant a = 375, 380 and 385 nm with a hole radius r = 0.298*a.

Due to the high conformity of the ALD, this dielectric layer is deposited uniformly over all the open surfaces of the NOEMS, including the bottom and the top parts of both membranes, as illustrated in Fig. 1(b). Figure 1(c) shows the effect of the coating on the effective refractive index of the structure as a function of the inter-membrane distance (d), calculated assuming the refractive index of alumina n_d = 1.615, as measured by spectroscopic ellipsometry. A small increase of the effective index, and therefore a red-shift, is expected for both the s- and the as- modes.

Optics EXPRESS

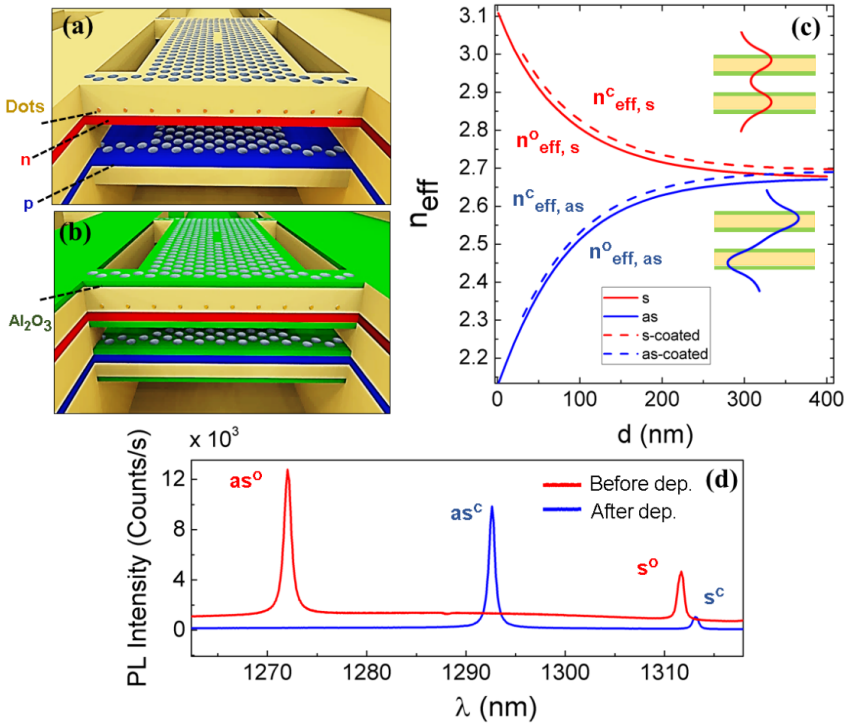

Fig. 1. Artistic sketches of the uncoated (a) and coated (b) NOEMS composed of two vertically-coupled PhC membranes. (c) Calculated effective refractive index of the symmetric (s) and anti-symmetric (as) modes, with ('o' superscript) and without ('c' superscript) coating. (d) Measured effect of the alumina coating on the optical properties of the photonic crystal cavity (device A). A red-shift with a different magnitude is observed for the fundamental s- and as- modes.

3. Results and discussion

Room temperature micro-photoluminescence (μPL) experiments have been carried out to study the influence of the anti-stiction coating on the static and dynamic properties of the device. In these experiments, the quantum dot layer is excited with a CW diode laser emitting at 650 nm with a power of 0.9 mW before the objective, above the bandgap of GaAs. The emission of the QDs, which is modulated by the local density of states of the PhC, is then collected through an objective (numerical aperture NA = 0.45) and analyzed by a spectrometer. A Ground-Signal-Ground probe is used to apply either a constant or a time-dependent bias to the cavity diode.

As a first set of experiments, we explore the effect of the dielectric coating on the optical properties of the NOEMS. Figure 1(c) shows the μPL spectrum of a PhC cavity (device A), collected before (red line), and after (blue line) the deposition of the alumina layer. The in-plane symmetry of the resonances shown Fig. 1(d) has been identified as the fundamental mode of the L3 cavity (labelled Y1), by a comparison with the eigenmodes obtained from FEM simulations [12], while the vertical profile is attributed to the symmetric (s) and anti-symmetric (as) modes, and further confirmed by the directions of the wavelength shift in electromechanical tuning experiments.

In general, the introduction of the alumina induces a red-shift of the spectrum for both modes as expected by the effect of a dielectric perturbation on the original resonances [18]. Since these two eigenmodes have the same in-plane symmetry - and therefore identical overlap with the alumina coating deposited inside the holes [18] - it is expected that the coating inside the holes produces a red-shift having similar magnitude, while the coating

Optics EXPRESS

between the membranes should produce a larger shift for the symmetric mode which has a larger field in the gap. However, the opposite is observed, namely the s-mode shows a smaller wavelength shift compared to the as-resonances. This can be explained by the fact that the deposition process induces a tensile stress on the membranes [19], which increases the inter-membrane distance and thus blue-shifts (red-shifts) the s-(as-)mode, thereby decreasing (increasing) the net red-shift produced. The average wavelength shift induced by the deposition of alumina, measured in three different devices having nominally identical mechanical properties, is $\Delta\lambda(as)=(22\pm3)$ nm and $\Delta\lambda(s)=(1.3\pm0.3)$ nm, where the error bar is the standard deviation.

In light of these observations, we write the wavelength change due to the alumina deposition as the sum of two contributions, $\Delta\lambda_{total}=\Delta\lambda_d+\Delta\lambda_m$, where $\Delta\lambda_m$ is due to the stress-induced mechanical deformation and $\Delta\lambda_d$ is due to the pure dielectric perturbation. These two contributions can be considered independent, since the change in the effective refractive index due to dielectric perturbation (Δn_{eff}) is practically independent of the distance for the inter-membrane distances investigated here (Fig. 1(c)).

In order to quantify these two wavelength shifts, we simulated the full-3D system using a commercial finite-element method (FEM) (Comsol). We assumed the nominal parameters of the structure, supposing that a layer of alumina of thickness t_d = 15 nm is conformally deposited on all the opened surfaces of the devices (above and below both membranes and inside the PhC pores). In this way, dielectric shifts of $\Delta\lambda_d^{FEM}(s)=15$ nm and $\Delta\lambda_d^{FEM}(as)=12.5$ nm are obtained for the s- and as- modes, respectively. The fact that $\Delta\lambda_d^{FEM}(s)>\Delta\lambda_d^{FEM}(as)$ is indeed due to the slightly larger field of the s-mode in the inter-membrane gap.

The remaining wavelength shift is attributed to the mechanical deformation of the structures ($|\Delta\lambda_m|$ = 10-14 nm). From FEM-simulations, we estimate a $\Delta d\sim100$ nm increase in the inter-membrane distance due to the induced mechanical stress. Note, that this analysis does not take into account a possible thickness difference between the membranes, which has been excluded by the inspection of cross-sectional scanning electron microscope images.

Interestingly, no degradation of the optical quality factors is observed. The average experimental quality factors of the fundamental as- and s- modes before the deposition are $Q_{exp}^{as,o}=1450\pm60$ and, respectively. These values are smaller compared to the Q-factors predicted by FEM simul $Q_{exp}^{s,o}=1900\pm170$ ations ($Q_{FEM}^{as,o}=1900$ and $Q_{FEM}^{s,o}=5700$), due to the presence of fabrication disorder. After the deposition, the Q-factors increase to $Q_{exp}^{as,c}=1810\pm50$ and $Q_{exp}^{s,c}=2300\pm300$. Notably, the calculated quality factors for the coated devices vary monotonically from $Q_{FEM}^{as,c}(d=200\text{ nm})=1700$ to $Q_{FEM}^{as,c}(d=300\text{ nm})=2480$ for the as-mode and, from $Q_{FEM}^{s,c}(d=200\text{ nm})=5740$ to $Q_{FEM}^{s,c}(d=300\text{ nm})=7160$ for the s-mode, due to the redistribution of the k-vector components inside the light cone [12]. Therefore, the increase in the quality factor observed can be associated to the aforementioned stress-induced mechanical reconfiguration of the devices.

3.1 Static actuation

In the following, we investigate the behavior of the NOEMS when a static electric potential is set between the two membranes. The wavelength of the anti-symmetric fundamental mode (*Y1as*) is used to track the mechanical state of the device B.

Optics EXPRESS

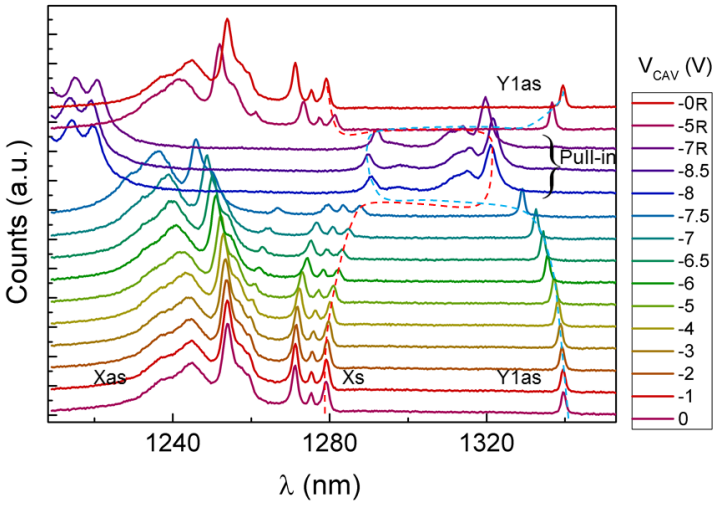

Fig. 2. Electromechanical tuning of the dual-membrane PhC cavity (device B). The cavity voltage is varied from 0 to −8.5 V and then back (label 'R') to 0 V. The pull-in instability appears as a jump in the photo-luminesce spectra at $V_{CAV} = -7.5$ V. The device can be operated back to the normal actuation when $V_{CAV} = -5$ V. The dashed lines are guides for the eye.

Figure 2 shows the tuning spectrum of the PhC modes as a function of the cavity voltage (V_{CAV}). Along with the fundamental as-mode (*Y1as*), other two sets of resonances appear in the spectra (labelled *Xas* and *Xs*), identified with higher-order modes of the double-membrane L3 cavity [12].

The device is firstly actuated from $V_{CAV} = 0$ V beyond the pull-in voltage (V_P ~-8V) and then back ('R') to 0 V. Three different regimes of operations (I, II, III) can be identified. During an initial phase (regime I) the PhC resonances red-shift or blue-shift depending on their vertical symmetry. This is caused by the continuous reduction of the inter-membrane distance under the application of the electrostatic force. The fundamental as-mode blue-shifts from $\lambda_{Y1as}(0\,\mathrm{V}) = 1339.5$ to $\lambda_{Y1as}(7.5\,\mathrm{V}) = 1328.9$ (i.e. by −10.6 nm). The value of the experimental tuning range is in good agreement with the observation that the initial inter-membrane distance is increased due to the stress-induced by the Al_2O_3 coating. In fact, from FEM simulations, when the gap between the membranes is reduced form $d_i = d_0 + \Delta d = 300$ = 300 nm to $d_f = 2/3\,d_i$, the expected tuning range for the Y1as-mode is $\Delta\lambda_{tun}^{th} = -11.6$ nm.

In general, the maximum tuning range measured before pull-in in the coated devices is reduced compared to the un-coated devices, due to the presence of stress-induced upward bending. In fact, a variation of the inter-membrane distance from d = 200 nm to d = 133 nm leads to a simulated change of the mode wavelength of 23 nm, while an experimental record tuning range of 30 nm has been obtained employing a different cavity design [20]. At pull-in, the PhC spectra change drastically (regime II). Here the modes experience an abrupt wavelength jump. In particular -after pull-in - the fundamental mode is located at $\lambda_{Y1as}(8\,\mathrm{V}) = 1290.32$ nm, resulting in a discrete blue-shift of $\Delta\lambda_{Pull-in}$ = 38.6 nm. From simulations, this corresponds to $d_{Pull-in}$~115 nm. The spectrum slightly changes for higher voltages, $|V_{CAV}| > V_{Pull\text{-}in}$, with a rate of ~1.0 nm/V. We repeated this tuning experiment on the same device in vacuum (p = 10^{-3} mbar). Here we obtained $\lambda_{Y1as}(-8\,\mathrm{V}) = 1268.7$ nm corresponding to a larger $d_{Pull-in}^{VAC} \sim 60.2$ nm nm and smaller distance at pull-in $d_{Pull-in}^{VAC} \sim 75$ nm, which corresponds to a residual spacing of ~ 45 nm between the alumina layers. As further discussed below, we attribute the non-zero value $d_{Pull-in}$ to the upward

Optics EXPRESS

bending of the top membrane, whereby peripheral parts of the structure get into contact first as the membranes are approaching. The difference in inter-membrane distance at pull-in in vacuum may be related to the different pressure dependent damping and thereby electromechanical dynamics, leading to a larger fraction of the structure being in contact. However, further investigation is needed to confirm this conclusion.

When the electro-mechanical voltage is decreased, the modes initially show small shifts, then below $V_{CAV} < V_{Pull\text{-}out}$ ~-5 V (regime III) they abruptly return to their initial wavelengths $\lambda_{Y1as}(0\,\mathrm{V}) = \lambda^{B}{}_{Y1as}(0\,\mathrm{V})$. We ascribe the difference in the pull-in and pull-out voltages ($V_{Pull\text{-}in} > V_{Pull\text{-}out}$) to the presence of a residual attractive force at contact.

We tested the tuning capabilities of 11 devices having a different bridge area ranging from 8 x 8 μm^2 to 8 x 12 μm^2. No permanent stiction was observed in any of the devices. The pull-in and pull-out voltages present an average $V_{Pull-in} = 7.4$ V and $V_{Pull-out} = 4.4$ V, and a root-mean-square variation of 0.7 V and 1.3 V, respectively. To further gain insight in the pull-in behavior (regime II), we employed a focused ion beam (FIB) setup equipped with two electrical needles (Fig. 3(a)), in order to visualize the cross-section of the device during the electromechanical actuation. Ion bombardment has been employed to etch a series of rectangular cuts at the center of the bridge through both membranes, as shown in Fig. 3(d), in order to open a view at the center of the bridge. We experimentally observed that for a small cut area A_1 = 3.4 x1.2 μm^2 the distance between the GaAs membranes varies from ~260 nm to ~40-60 nm, when a device (device C) is operated from 0 V to above pull-in (Fig. 3(b,c)). The non-zero inter-membrane distance is in agreement with the value derived from the optical measurements. The same experiment is repeated after increasing the area of the cut to A_2 = 12.0 x 1.2 μm^2. In this configuration, when the membranes are brought to pull-in, a full contact between the two slabs is achieved, as shown in Fig. 3(d,e). When the voltage is set back to 0 V, the membranes return back into their original position (Fig. 3(f)).

These experiments indicate that the presence of internal stress produced during the coating of the chip bends the central region of the bridge upwards with respect to the peripheral parts of the structure. By opening a large area at the center of the bridge, the internal stress is released and full contact can be achieved in this region.

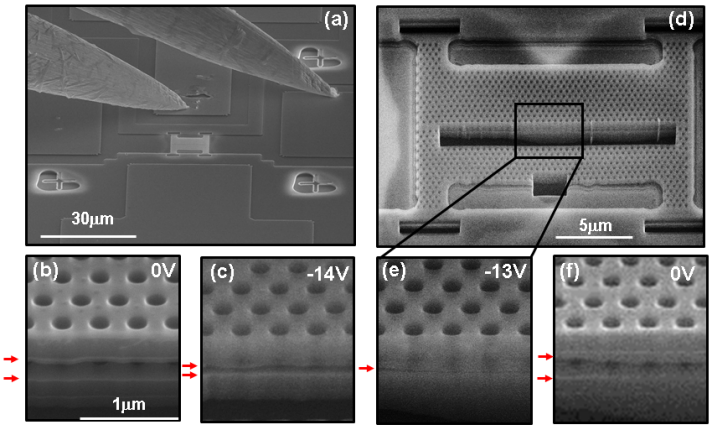

Fig. 3. Investigation of the static pull-in via cross-section scanning electron images analysis. (a) Tilted SEM view of the device along with a pair of needles employed for the cavity actuation. (b) and (c) SEM cross-sections, when V_{CAV} is set to 0 V and −14 V, respectively. (e) and (f) cross-sectional SEM images, after opening a large cut at the center of bridge (d) when the device C is operated from −13 V to 0 V, respectively. The red arrows indicate the positions of the membranes. Note, that the layer of alumina is visible and thicker than the one measured by ellipsometry due the re-deposition of this material during the FIB cut.

Optics EXPRESS

3.2 Dynamic actuation

In order to investigate the reliability of the tuning for applications that require digital switching between the rest and the pull-in state [19], the device A has been actuated for more than 1000 cycles from 0 to 10 V, with a square-wave signal having a period T = 1 s. No degradation of the PhC quality factors has been observed as shown in Fig. 4 (bottom). A small wavelength shift, comparable to the resolution of the spectrometer (0.32 nm), is observed after 1000 cycles when the cavity voltage is set to 0 V.

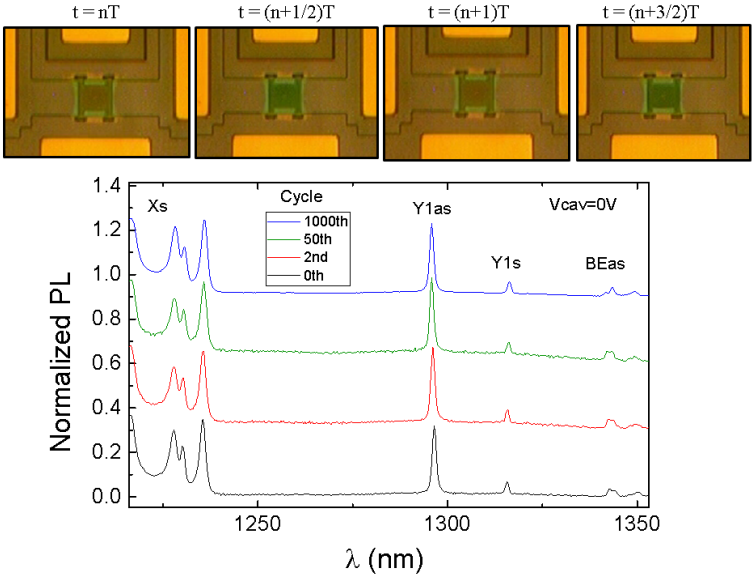

Fig. 4. (Top) Optical microscope images of the device A when it is actuated from 0 V (release) to −10 V (pull-in) with a period T = 1s. (Bottom) PL spectra of the L3 cavity after 0, 2, 50 and 1000 cycles.

Figure 4 (top) shows the optical microscope images recorded while the device was actuated between the pull-in and release configuration. Here, the color of the bridge (red/green) arises from the thin-film interference in the reflection from the membranes when it is either in the pull-in or in the release state.

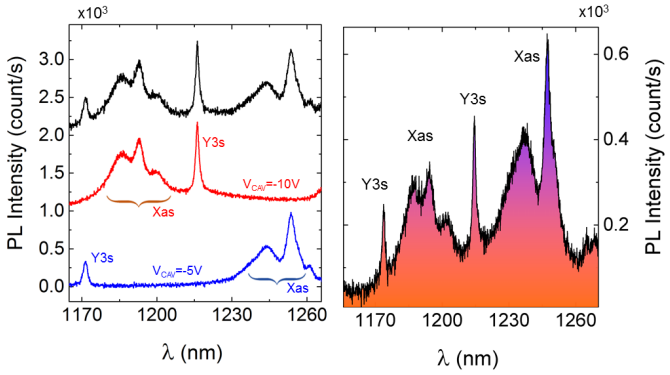

Fig. 5. Operation of the PhC NOEMS (device B) as a digital switch between two opto-mechanical states. (left) PhC modes during the static actuation. The blue and the red curves correspond to the PL spectra acquired at $V_{CAV} = -5V$ and $V_{CAV} = -10V$, respectively, while the black curve represents their sum.(right) PL spectra from pull-in to release status integrated over 500,000 cycles with a modulation frequency of 100 kHz.

Optics EXPRESS

In order to investigate the optical properties of the device during an even larger number of actuation cycles, we measured the PL spectra of the NOEMS integrated over the modulation experiment (device B). To this end, device B was actuated in vacuum (pressure $p = 10^{-3}$ mbar) from $V_{CAV} = V_i = -5\,\mathrm{V}$ to $V_{CAV} = V_f = -10\,\mathrm{V}$ with a square-wave voltage of frequency $f = 100$ kHz and 50% duty-cycle. In what follows, we present the results for the higher order cavity mode, labelled Y3s, that - differently from the fundamental Y1as (see Fig. 2) - does not overlap with any modes in the spectra range after pull-in. Figure 5 (right panel) shows the PL spectrum integrated over 0.5 million modulation cycles at 100 kHz. Here, the set of modes labelled Xas and Y3s can be recognized by comparison with the sum of the spectra (Fig. 5, left panel, black curve) collected in the static configurations at the two voltage values (V_i, V_f) (Fig. 5, left panel, red and blue curves). The range of the wavelength modulation for the mode Y3s is 41.2 nm. The fact that the modes Y3s and Xas in the PL spectra obtained during static actuation can be distinctly identified in this modulation experiment indicates that the initial and the final mechanical positions of the membranes are identical for different modulation cycles. Importantly, no degradation is observed in both the quality factor ($Q(Y3) \sim 1000$) and the PL intensity of the modes.

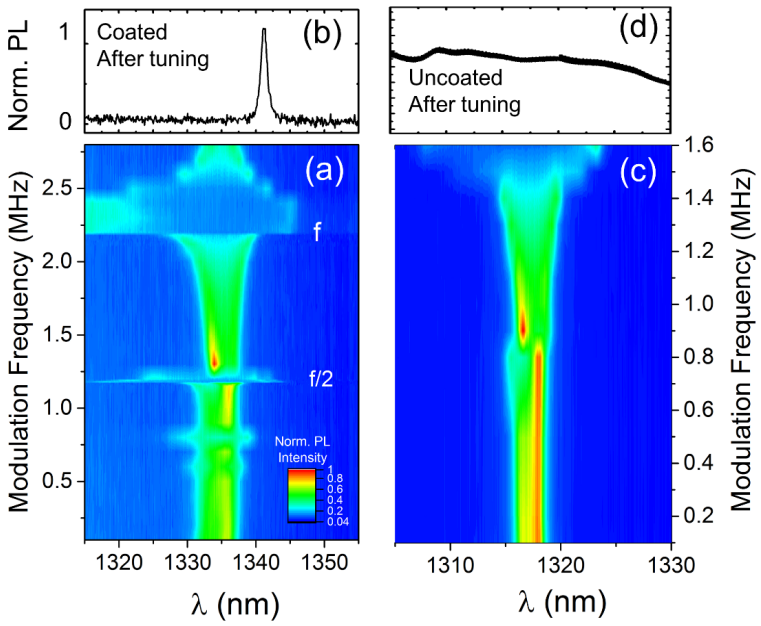

Fig. 6. Dynamical modulation experiment carried on a coated (a,b) and an uncoated (c,d) NOEMS. (a) and (c) photo-luminescence color-coded map obtained under the application of an AC bias for a coated and uncoated device, respectively.(b) and (d) normalized PL spectra of the unbiased coated and uncoated devices, respectively, collected after the modulation experiment.

Finally, we investigated the dynamic modulation of the coated NOEMS when it is operated under a strong AC signal with varying frequency, in order to study the pull-in dynamics in the presence of the coating [7, 8, 11]. A DC bias $u_{DC} = -6\,\mathrm{V}$ together with an AC sinusoidal component of amplitude $u_{AC} = 1\,\mathrm{V}$ were used to excite the cavity diode.

Figure 6(a) shows the color-coded experimental μPL data of the mode Y1 as collected while varying the frequency (f) of the AC sinusoidal modulation from 0.1 MHz to 2.8 MHz. At low frequencies, the spectrum is characterized by a broad peak centered at $\hat{\lambda} = 1334.7$ nm, featuring a full width half-maximum (FWHM) of 5.5 nm. The minimum and maximum

Optics EXPRESS

wavelengths of this peak correspond to the static wavelength positions at $\lambda(V_{CAV} = -7V) = 1331.7$ nm and $\lambda(V_{CAV} = -5V) = 1337.2$ nm displayed in Fig. 2. The maximum of the PL intensity is red-shifted compared to $\hat{\lambda}$ as expected by the non-linearity of the tuning. When the modulation frequency equals the mechanical frequency of the structure, a broadening of the spectrum is expected due to the amplification of the membrane oscillations. Indeed, a drastic broadening of more than 30 nm in the PL peak is observed at f = 2.3 MHz, which is close to the calculated mechanical frequency of f_{th} = 2.2 MHz. Since the electrostatic force has a quadratic dependence on the actuation voltage, a broadening at $f/2$ is also visible. We note, that below 1 MHz mechanical modes are not expected from FEM simulations and have not been observed in experiments employing small modulation amplitudes [11]. Yet, we speculate that the broadening of the experimental PL below 1 MHz can be due to non-linear high-order terms in the elastic force in this strong modulation regime. The cavity spectrum of the unbiased device after the modulation experiment is plotted in Fig. 6(b). It is worth mentioning that in less critical experimental conditions ($u_{DC} > -2$ V, $u_{AC} = -1$V), the collapse of the structures is observed for 3 uncoated devices produced in the same fabrication run with a 100% failure probability. For comparison, an example of a dynamical tuning curve ($u_{DC} = -2$ V, $u_{AC} = -1$V) of an uncoated device with similar structural parameters is shown in Fig. 6(c). In this experiment the device does not recover from the instability occurring at f~1.6 MHz: a permanent collapse of the structure is observed, as verified by the absence of a cavity mode in the broadband emission spectra collected after the tuning experiment (Fig. 6(d)). These results clearly indicate that the coating prevents the structure from permanent collapse also when the device is modulated with a frequency comparable to its natural frequency and allows the switching between two mechanical and optical states up to MHz rates.

4. Conclusions

Pull-in and stiction failure are often considered detrimental effects in the operation of NOEMS. Here, we have demonstrated a method based on the atomic layer deposition of alumina that prevents the stiction failure after pull-in of mechanically-tunable photonic crystal membranes.

The operation of the device as a static and dynamic optical switch is demonstrated, with the possibility to reversibly modulate the wavelength of a PhC mode over ~50 nm.

These results not only represent a crucial step towards real-world applications of this current NOEMS, but also open the way to new devices that exploit the intrinsic non-linearity of the pull-in to achieve digital optical switching and mechanical memories.

Funding

Dutch Technology Foundation STW; Netherlands Organization for Scientific Research (NWO) Applied Science Division; Technology Program of the Ministry of Economic Affairs (10380 and 12662); The Dutch Ministry of Education, Culture and Science under Gravity Program “Research Centre for Integrated Nanophotonics”; Research Program ’Nanoscale quantum optics’ of the Foundation for Fundamental Research on Matter (FOM).

Acknowledgments

The nanofabrication used in this work has been performed in the NanoLab@TU/e cleanroom. We acknowledge stimulating discussions with Dr. H.C.M. Knoops.